dc probe detection of phased EEDFs in RF discharges

Francis F Chen

Electrical Engineering Department, University of California, Los Angeles, CA 90024-1594, USA

Abstract. Detection of non-Maxwellian electron energy distribution functions (EEDFs) by Langmuir probes in the presence of radiofrequency (RF) fluctuations in the plasma potential is possible if the probe is properly RF compensated. If the non-thermal electrons are created by wave acceleration, however, they usually are bunched at one phase of the RF. In this case, the usual method of forcing the probe to follow fluctuations in the floating potential (V_f) will be inappropriate, since V_f itself will be time-dependent in such a way as to ensure that the fast electron tail is not detected. The probe must be made to follow fluctuations in the *space* potential. Computations are given to show the effect of a RF on distributions with high-energy tails with and without the proper compensation. Singular EEDFs arising in the case of constant energy gain are also treated for the first time.

1. Introduction

In some radiofrequency (RF) plasma sources, such as the helicon source [1], it has been suggested that the ionizing electrons could be accelerated by wave–particle interactions [2]. In this case, the fast electrons, of the order of 50–100 eV, would be bunched in the accelerating phase of the wave's parallel electric field E_z, where z is the direction of the dc magnetic field B_0, as shown in figure 1. The occurrence of such bunched electrons has been inferred from the observed time variation of optical light emission in synchronism with the RF [3]. To detect these electrons with a simple diagnostic such as a Langmuir probe requires careful RF compensation to remove the nonlinear averaging imposed by large RF fluctuations in the plasma potential. Many methods for doing this can be found in the literature on RF plasma sources. For instance, the method developed by Sudit and Chen [4] employs RF chokes to filter the fundamental and first harmonic of the RF frequency and, in addition, a large auxiliary floating electrode to sense the voltage fluctuations near the probe tip and to couple them to the tip, causing it to follow the fluctuations. Unfortunately, the floating potential itself is affected by the fast electrons, in such a way that V_f shifts negatively whenever the fast electrons are collected. The result is that the RF compensation is too strong and guarantees that the electron tails cannot be seen on the probe characteristics. This is true of any RF probe method which relies on feeding back a floating potential signal. An ideal probe would sense the local *space* potential V_s and use that for RF feedback, thus avoiding the self-masking aspect of phased beams. At this time we do not know of an easy way to do this.

In this paper, we compute the probe characteristics for typical discharges with various levels of RF noise and with various fast electron tails, phased and unphased. The effects of insufficient, perfect, and excessive RF compensation are calculated. These current–voltage (I–V) curves are similar to those shown previously by others [5] but are somewhat more
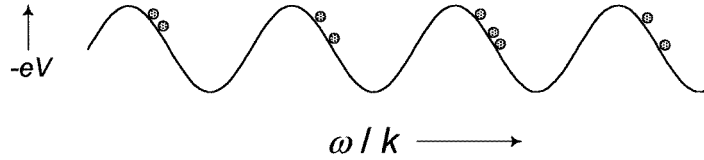
Figure 1. The electric potential seen by electrons, showing their bunching at the phase of a propagating wave at which there is an accelerating electric field.

realistic in that the rounded 'knee' observed in the presence of strong magnetic fields is reproduced in the computations. In addition, a distribution of fast electrons other than a shifted Maxwellian is also treated; this is the case of singular electron energy distribution functions (EEDFs) which arise if the energy gain of the fast electrons, rather than their velocity gain, is constant. The ideas conveyed here are general enough to be applicable to any RF discharge in which the electron distribution function varies at the RF frequency. Although we have implied the existence of a magnetic field in order to use a simple one-dimensional electron distribution, this simplification is not essential.

2. Formulation

Let V_p be the probe bias voltage and V_s the space, or plasma, potential. We neglect oscillations in plasma density and temperature but allow V_s to vary sinusoidally at the RF frequency:

$$V_s = V_{rf} \cos \omega t. \tag{1}$$

The probe potential relative to the plasma is defined as V:

$$V \equiv V_p - V_s. \tag{2}$$

The minimum velocity of an electron that can reach the probe is then given by

$$\tfrac{1}{2} m v_m^2 = -eV. \tag{3}$$

Hence,

$$v_m = (-2eV/m)^{1/2} \qquad v_m^2/v_e^2 = -eV/KT_e. \tag{4}$$

Let the bulk plasma electrons be Maxwellian with temperature T_e, and let the ions be cold. We consider the one-dimensional case, in which the normalized electron velocity distribution is

$$f_e(v) = (1/v_e\sqrt{\pi}) \exp(-v^2/v_e^2) \tag{5}$$

where

$$v_e \equiv (2KT_e/m)^{1/2} \qquad \bar{v}_e \equiv v_e/2\sqrt{\pi}. \tag{6}$$

Added to this is a population of fast (beam) electrons of density n_b, whose distribution will be discussed later. The densities at the sheath edge are related by

$$n_i = n_e + n_b. \tag{7}$$

2.1. Thermal electron current

For $V < 0$, the thermal electron flux collected by the probe is

$$j_e = n_e \int_{v_m}^{\infty} v f_e(v) \, dv = (n_e v_e / 2\sqrt{\pi}) \exp(-v_m^2/v_e^2) = n_e \bar{v}_e \exp(eV/KT_e). \tag{8}$$

Defining the dimensionless variables

$$J = j/n_e \bar{v}_e \qquad \eta = eV/KT_e \tag{9}$$

we can write (8) as

$$J_e = e^{\eta}. \tag{10}$$

For $V > 0$, J_e is replaced by its saturation value J_{sat}. In a strong magnetic field, the probe's presence necessarily changes the plasma potential on the flux tube that it blocks, and saturation starts well before $V_p - V_s = 0$, if V_s is referred to the plasma on undisturbed flux tubes. For the purposes of this paper, it is sufficient to model the saturation current with a two-parameter curve (a parabola) that resembles the I–V characteristics seen experimentally. Let a be the value of J_e at which saturation begins, and let b describe the rate at which the saturation current grows. Matching the slope of the parabola to that of equation (10) at $J_e = a$, we obtain

$$J_{sat} = a - b^2/2a + b[\eta - \ln a + (b/2a)^2]^{1/2}. \tag{11}$$

The potential η_c at the onset of saturation is given by $\eta_c = \ln a$. Thus, the thermal electron current is given by

$$J_e = \begin{cases} e^{\eta} & \eta < \eta_c \\ J_{sat} & \eta > \eta_c. \end{cases} \tag{12}$$

2.2. Ion current

The normalized saturation ion current is approximately [5]

$$J_i \approx 0.5 \frac{n_e + n_b}{n_e \bar{v}_e} \left(\frac{KT_e}{M} \right)^{1/2} = (1 + f) \left(\frac{\pi m}{2M} \right)^{1/2} \tag{13}$$

where M is the ion mass. In practice, the ion current varies slowly with voltage and can be approximated by a parabola. Since the exact ion current is not critical here, we arbitrarily set it to have the value in (13) at a probe potential of $-36 \, KT_e$. Thus we take the normalized ion current to be

$$J_i = (1 + f) \left(\frac{\pi m}{2M} \right)^{1/2} \frac{\sqrt{-\eta}}{6}. \tag{14}$$

2.3. Electron beam current

The normalized probe current J_b due to accelerated 'beam' electrons will be derived in the next section, giving a total probe current

$$J = J_e + J_b - J_i. \tag{15}$$

3. Beam distributions

The distribution function of the non-thermal electrons depends on the acceleration mechanism. We assume that the accelerated electrons are concentrated at the phase of the RF at which the electric field has the proper sign and is at its maximum so that its magnitude is insensitive to phase. A runaway population of these electrons can be defined as those which are quickly accelerated well above their thermal speeds before making a collision. These electrons will experience the electric field until they fall out of phase or make a collision with an ion or a neutral atom. We assume that the collisional mechanism prevails. If their collision cross section varies as $1/v$, then the collision frequency will be constant, and the electrons will, on average, be accelerated for a time equal to $1/n_o \sigma v$, where n_o is the density of scattering centres. In this case, the velocity gained by each electron will be the same regardless of its initial velocity, and the EEDF is that of a shifted Maxwellian, the case usually treated. On the other hand, if the cross section is constant, the electrons will, on average, be accelerated for a given distance; namely, the mean free path $\lambda_m = 1/n_o \sigma$. This distance is approximately constant for a distribution of about 3 eV width accelerated to 50–100 eV. In this case, the *energy* gained by each electron will be the same, leading to a different EEDF. We have calculated the probe currents for these two extremes; the actual distribution will probably lie in between. One-dimensional distributions are used, since the magnetic field has been assumed strong enough that even the beam electrons move primarily in the z direction.

3.1. Shifted Maxwellian

At the sheath edge, the distribution function of a Maxwellian of temperature T_b shifted by a velocity u is

$$f_b(v) = (1/v_b\sqrt{\pi}) \exp[-(v-u)^2/v_b^2] \tag{16}$$

where

$$v_b \equiv (2KT_b/m)^{1/2} \qquad \bar{v}_b \equiv v_b/2\sqrt{\pi}. \tag{17}$$

The beam current is then

$$j_b = \frac{n_b}{v_b\sqrt{\pi}} \int_{v_m}^{\infty} \exp[-(v-u)^2/v_b^2]v \, dv. \tag{18}$$

This yields

$$j_b = n_b\bar{v}_b[\exp(-y_m^2/v_b^2) + (u/v_b)\sqrt{\pi}\, \text{erfc}(y_m/v_b)] \tag{19}$$

where $y_m = v_m - u$ (equation (4)), $\text{erfc}(x) = 1 - \text{erf}(x) = 1 + \text{erf}(-x)$, and

$$\text{erf}(x) = \frac{2}{\sqrt{\pi}} \int_0^x e^{-t^2} \, dt. \tag{20}$$

In terms of the dimensionless quantities

$$f \equiv n_b/n_e \qquad h \equiv v_b/v_e \qquad q \equiv u/v_b \tag{21}$$

the normalized beam current can be written

$$J_b = j_b/n_e\bar{v}_e = fh[\exp(-Y_m^2) + q\sqrt{\pi}\, \text{erfc}(Y_m)] \tag{22}$$

where

$$Y_m = \begin{cases} y_m/v_b = (-\eta)^{1/2}/h - q & \eta < 0 \\ -q & \eta > 0. \end{cases} \tag{23}$$

This assumes that the fast electrons saturate above the space potential. The initial and final distributions are sketched in figure 2; the 'final' distribution is that found at the sheath edge, before it is changed by the sheath electric field.
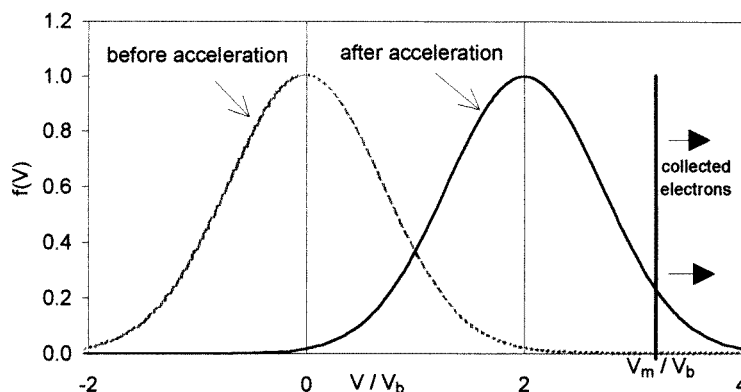

Figure 2. The beam distribution functions before and after wave acceleration, for the case of constant velocity gain. Electrons faster than v_m are able to overcome the probe bias.
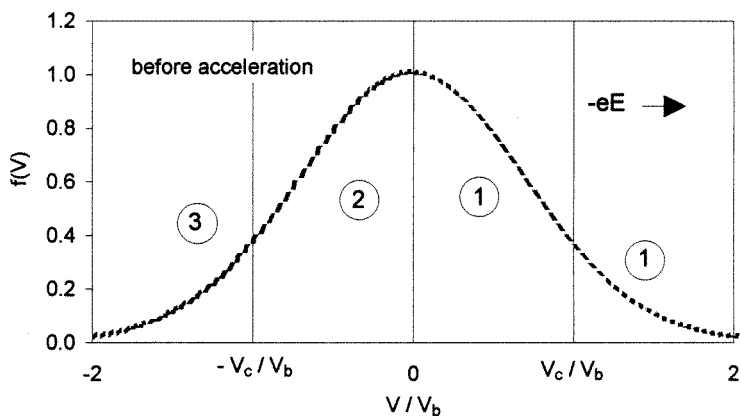

Figure 3. Velocity regions of a Maxwellian beam distribution before each electron is given an energy $W = mv_c^2/2$.

3.2. Constant energy case

In this case, let the beam distribution start as a Maxwellian at temperature T_b, and let each accelerated electron gain or lose an energy W. The centre of the velocity distribution will then be shifted by an amount v_c, where

$$v_c = (2W/m)^{1/2}. \tag{24}$$

The initial distribution is divided into three regions, as shown in figure 3. Those electrons originally moving in the direction of the acceleration will gain an energy W; those originally moving fast in the opposite direction will lose an energy W; and those moving slowly in
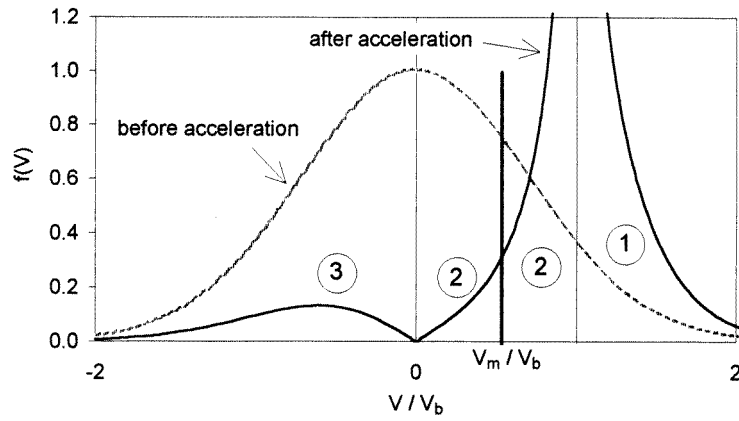
Figure 4. The beam distribution after acceleration in the constant-energy case. The numbered regions correspond to those in figure 3. Electrons with $v > v_m$ reach the probe.
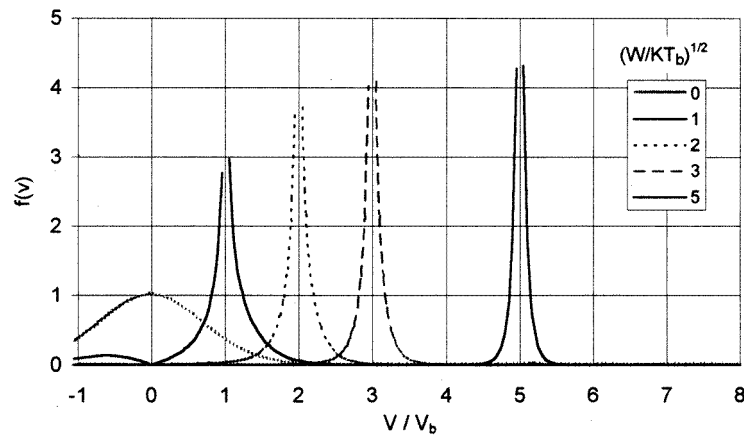

Figure 5. Velocity distribution of beam electrons in the case of constant energy gain W, for various values of W/KT_b.
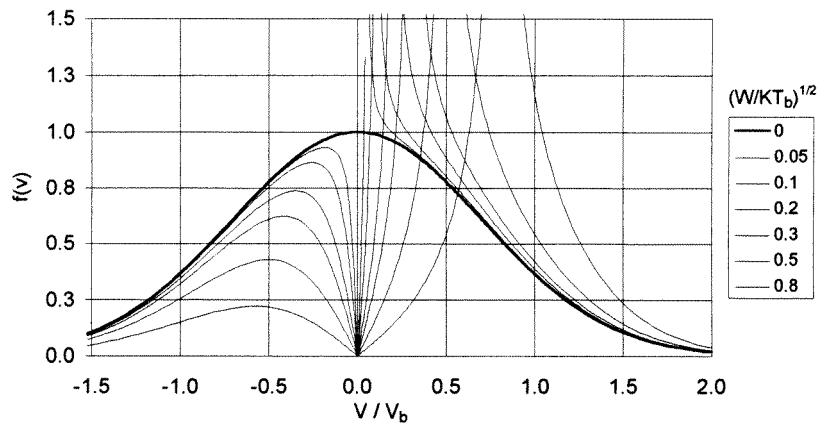

Figure 6. Velocity distribution of beam electrons for small energy gains, showing the development of the singularity in $f(v)$.
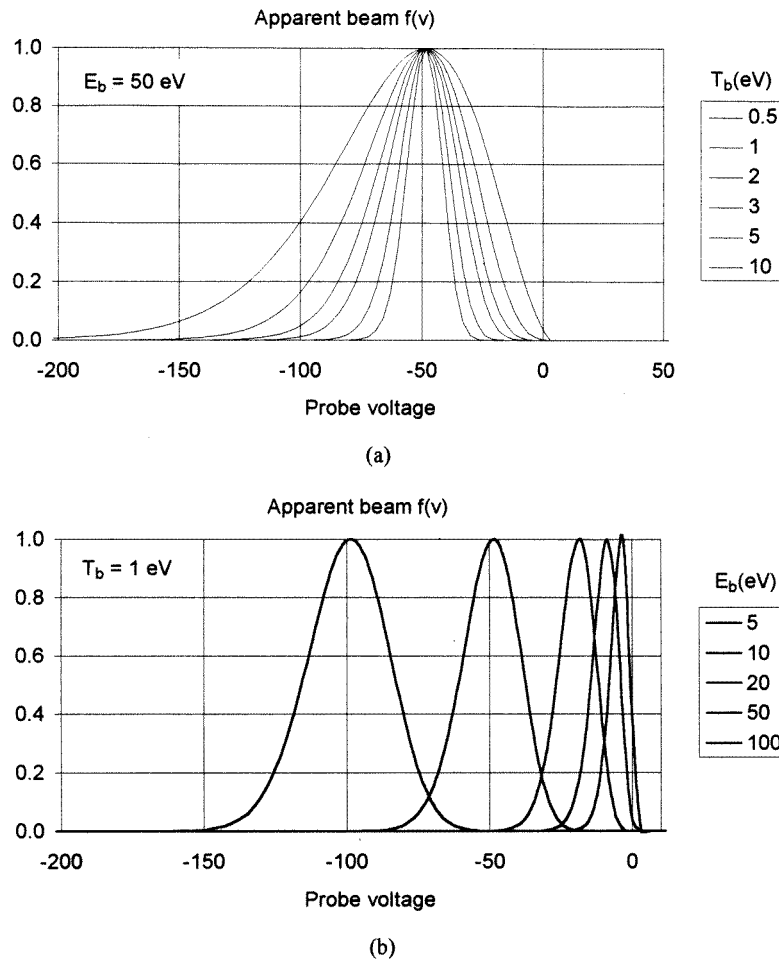
Apparent beam f(v)

(a)

Apparent beam f(v)

(b)

Figure 7. Apparent velocity distributions of electrons in a shifted Maxwellian for (a) various beam temperatures and (b) various velocity shifts. These curves are obtained by differentiating the probe *I–V* curves and are therefore plots of $f(v)$ against v^2.

the backward direction will be turned around. The final velocity v of an electron with initial velocity v_0 is thus given by

(Region 1) $\quad v_0 > 0:\qquad v^2 = v_0^2 + v_c^2 \qquad (v > 0)$ $\hfill$ (25a)

(Region 2) $\quad -v_c < v_0 < 0:\qquad v^2 = v_c^2 - v_0^2 \qquad (v > 0)$ $\hfill$ (25b)

(Region 3) $\quad v_0 < -v_c:\qquad v^2 = v_0^2 - v_c^2 \qquad (v < 0).$ $\hfill$ (25c)

These regions, shown in figure 3, map into the corresponding regions of the accelerated distribution in figure 4.

Region 1. We have

$$v_0^2 = v^2 - v_c^2 \qquad \mathrm{d}v_0 = (v/v_0)\,\mathrm{d}v. \tag{26}$$
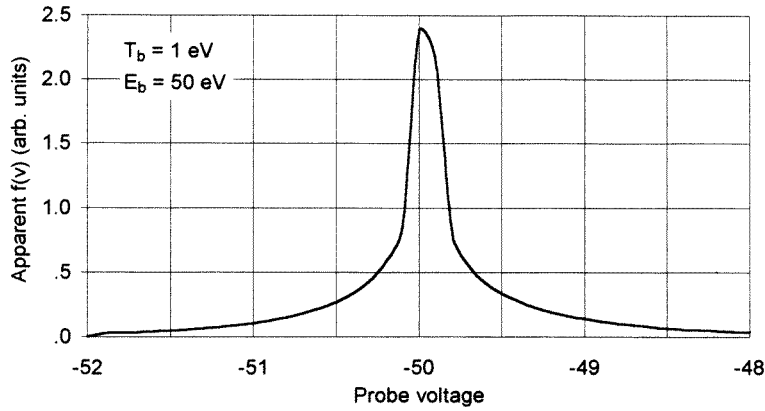
Taking

$$f_0(v_0)\,\mathrm{d}v_0 = f(v)\,\mathrm{d}v$$

Figure 8. Apparent velocity distribution of electrons accelerated by a constant energy W. This curve is obtained by differentiating the probe I–V curve and, therefore, the apparent width depends on the resolution of the computation.
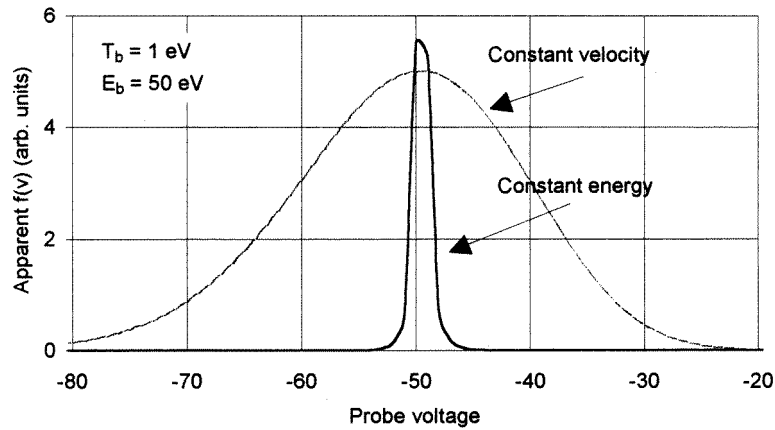

Figure 9. Apparent velocity distributions of a 1 eV electron distribution, after acceleration by the same mean energy, in the constant-velocity and constant-energy cases. The remarks under figures 7 and 8 apply.

with $f_0(v_0)$ given by equation (16), we obtain

$$f(v) = \frac{1}{v_b\sqrt{\pi}} \frac{v}{(v^2 - v_c^2)^{1/2}} \exp[-(v^2 - v_c^2)/v_b^2]. \tag{27}$$

Note that $f(v)$ has an integrable singularity at $v = v_c$. That accelerated distributions can be singular is well known [6]. The physical reason for this is that $f_0(v_0)$ has zero slope at v_0, so that these particles, which end up at $v = v_c$, are bunched into an infinitesimally small velocity interval. Similarly, the Jacobean dictates that $f(v)$ has to vanish at $v = 0$. Integrating $f(v)$ from v_c to ∞, we find that the fraction of particles in this region is $\frac{1}{2}$, as expected.

Region 2. Now we have

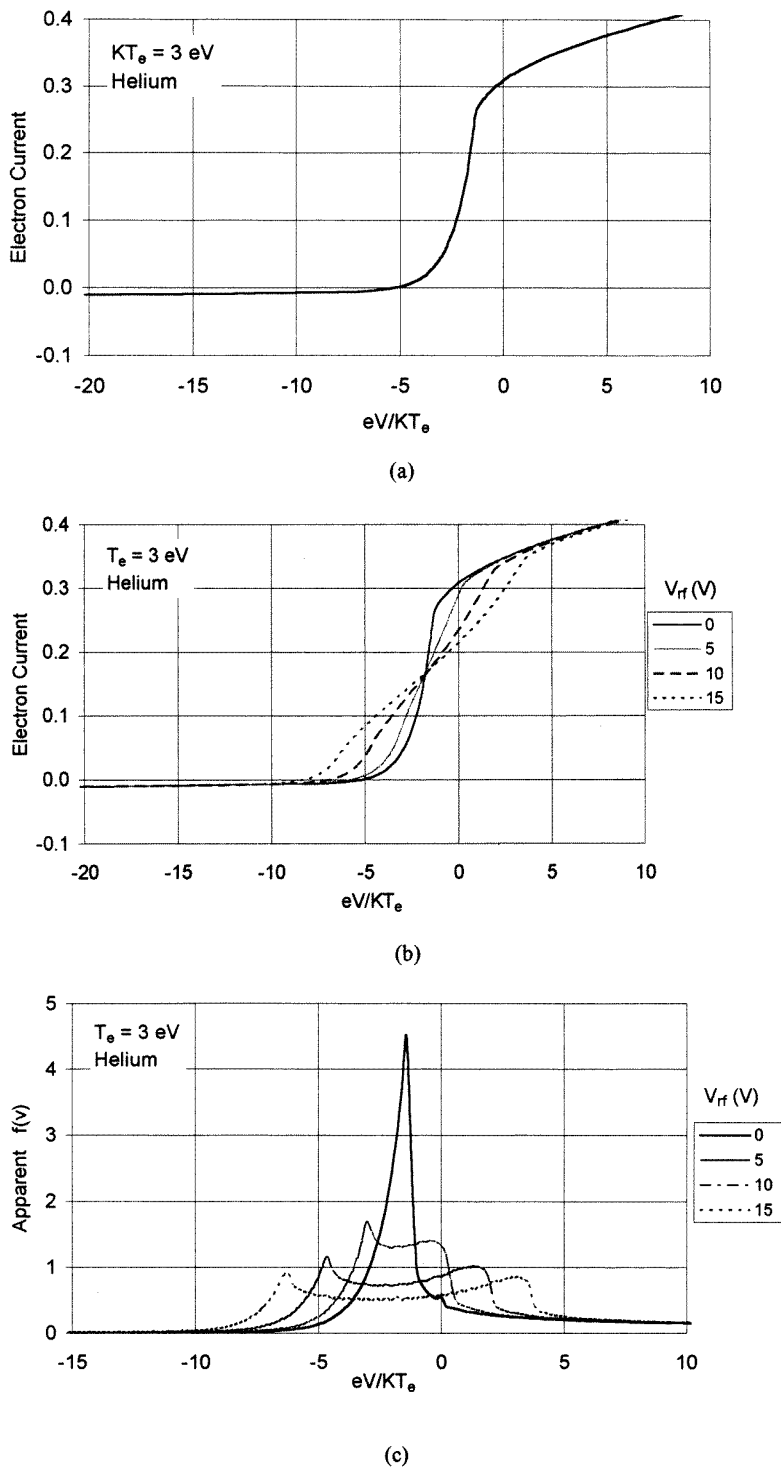$$v_0^2 = v_c^2 - v^2 \qquad dv_0 = -(v/v_0)\, dv. \tag{28}$$

(a)

(b)

(c)

Figure 10. (a) Normal I–V characteristic for a $T_e = 3$ eV, $T_i = 0$ Maxwellian plasma in a magnetic field. (b) The I–V curve of (a) after distortion by RF oscillations of magnitude V_{rf}. (c) Derived velocity distribution $f(v)$ against normalized probe voltage.
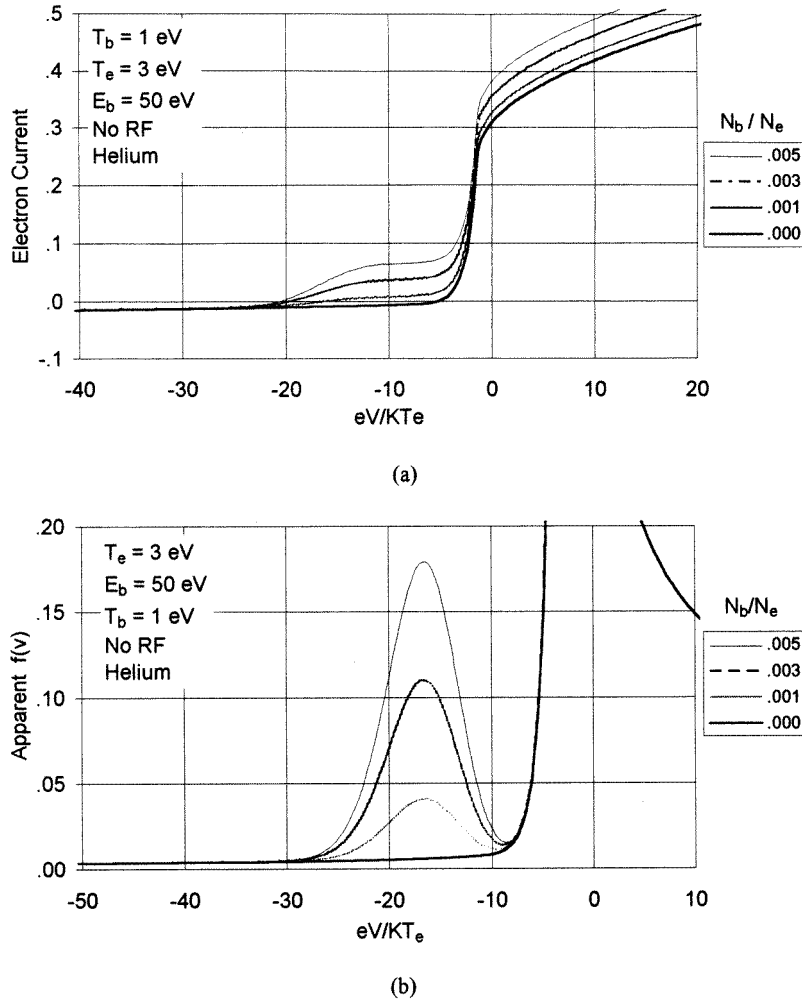
(a)

(b)

Figure 11. (a) *I–V* characteristics for a 3 eV plasma with a $T_b = 1$ eV beam of various densities. (b) Apparent distributions $f(v)$ derived from (a). (c) Apparent $f(v)$'s for a plasma with 50 eV beams of various temperatures. The *I–V* curves from which these were derived are not shown. (d) Apparent $f(v)$'s for a plasma with beams of the same density but different energies.

This gives

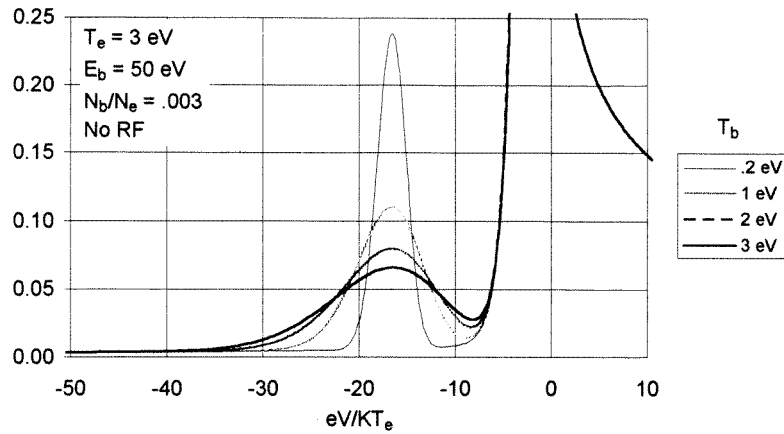$$f(v) = \frac{1}{v_b\sqrt{\pi}} \frac{v}{(v_c^2 - v^2)^{1/2}} \exp[-(v_c^2 - v^2)/v_b^2]. \tag{29}$$

The fraction of particles in this region is $\frac{1}{2}\,\text{erf}(v_c/v_b)$.
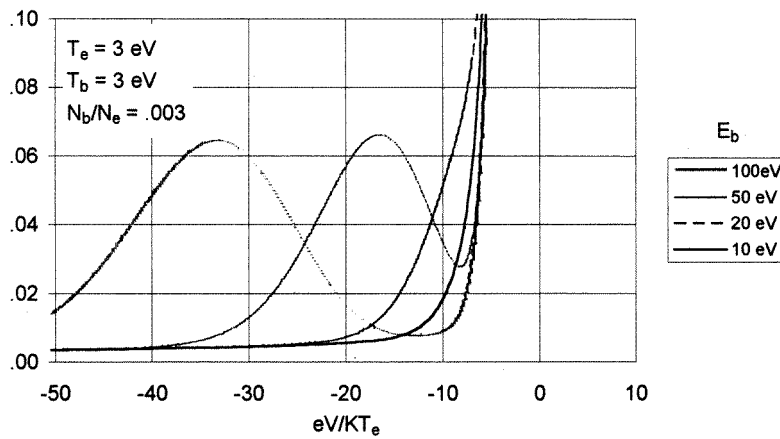
Region 3. In this case, we have

$$v_0^2 = v_c^2 + v^2 \qquad dv_0 = (v/v_0)\,dv \tag{30}$$

so that

$$f(v) = -\frac{1}{v_b\sqrt{\pi}} \frac{v}{(v^2 + v_c^2)^{1/2}} \exp[-(v^2 + v_c^2)/v_b^2]. \tag{31}$$

(c)

(d)

Figure 11. (Continued)

The fraction of particles in this region is $\frac{1}{2}\operatorname{erfc}(v_c/v_b)$, where erfc is the complementary error function. Figure 5 shows $f(v)$ for various values of W, and figure 6 traces how the zero and pole in $f(v)$ develop as a Maxwellian distribution is given a small energy gain.

The current of fast electrons to the probe is given by

$$j_b = n_b \int_{v_m}^{\infty} v f(v)\, dv. \tag{32}$$

If v_m is larger than v_c, the integral lies within region 1, and $f(v)$ is given by equation (26). The normalized collected beam current is then

$$J_b = \frac{f h}{\sqrt{\pi}} \int_{Y_m}^{\infty} (y^2 + q^2)^{1/2} \exp(-y^2)\, dy \qquad (v_m > v_c) \tag{33}$$

where

$$y = (v^2 - v_c^2)^{1/2}/v_b \qquad Y_m = (v_m^2 - v_c^2)^{1/2}/v_b = (-\eta/h^2 - q^2)^{1/2}. \tag{34}$$
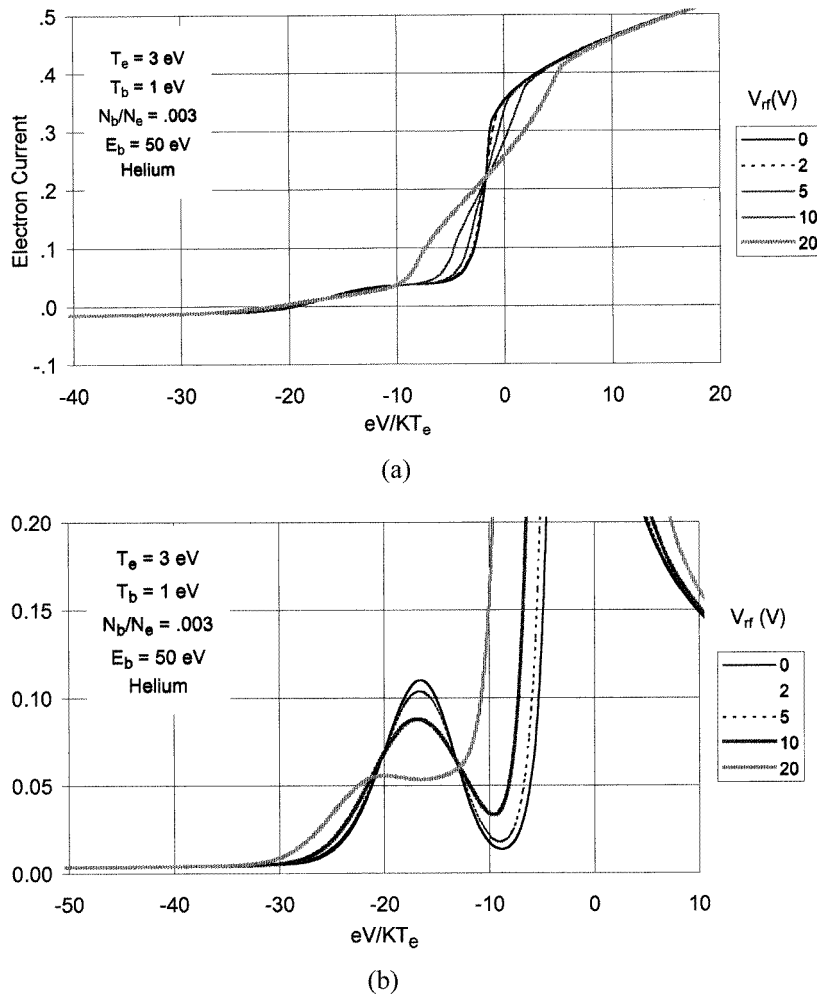
(a)

(b)

Figure 12. (a) Probe characteristics for a plasma with a dc beam after distortion by various amounts of RF pickup. (b) The apparent distribution function in the region of the beam obtained by differentiation of the curves in (a).

If v_m is smaller than v_c, part of the distribution lies in region 2, and equation (28) has to be used for that part. The result is

$$J_b = \frac{fh}{\sqrt{\pi}} \left[\int_0^{Y_m} (q^2 - y^2)^{1/2} \exp(-y^2)\,\mathrm{d}y + \int_0^{\infty} (q^2 + y^2)^{1/2} \exp(-y^2)\,\mathrm{d}y \right] \qquad (v_m < v_c) \tag{35}$$

where, in the first integral,

$$y = (v_c^2 - v^2)^{1/2}/v_b \qquad Y_m = (v_c^2 - v_m^2)^{1/2}/v_b = (\eta/h^2 + q^2)^{1/2}. \tag{36}$$

In this case, saturation occurs for $\eta > 0$, and Y_m has a maximum value of q.

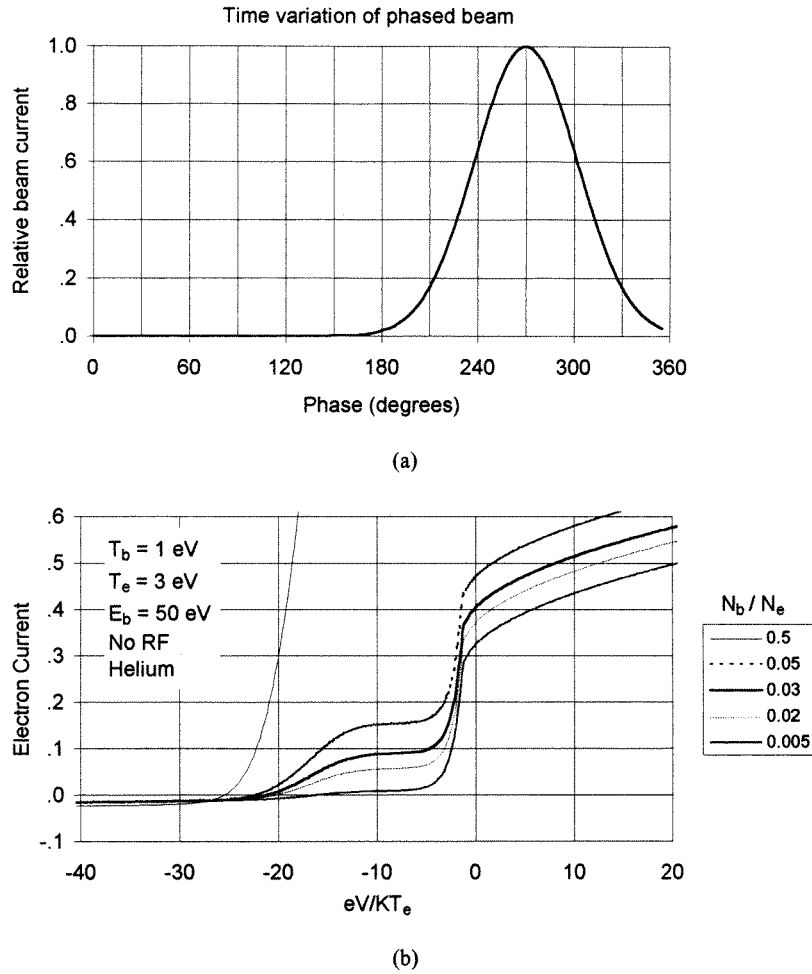## Time variation of phased beam

(a)

(b)

Figure 13. (a) Time variation of phased electron beams used in the calculations. (b) Probe characteristics for a 3 eV plasma with a phased beam of various peak densities in the absence of RF pickup and of RF compensation circuitry.

3.3. Recovery of $f(v)$

For three-dimensional distributions, $f(v)$ is proportional to the second derivative of the probe current; but in strong magnetic fields, the electron motion is one-dimensional, and $f(v)$ is given by the first derivative

$$j_e = n_e \int_{v_m}^{\infty} v f(v) \, dv \qquad dj_e/dv_m = -n_e v_m f(v_m) \qquad dj_e/dV = n_e(e/m) f(v_m) \quad (37)$$

where equation (4) was used for v_m. In terms of the dimensionless quantities J and η (equation (9)), we have

$$f(v_m) = \frac{1}{v_e \sqrt{\pi}} \frac{dJ}{d\eta}. \qquad (38)$$

For a shifted Maxwellian, equation (22) gives

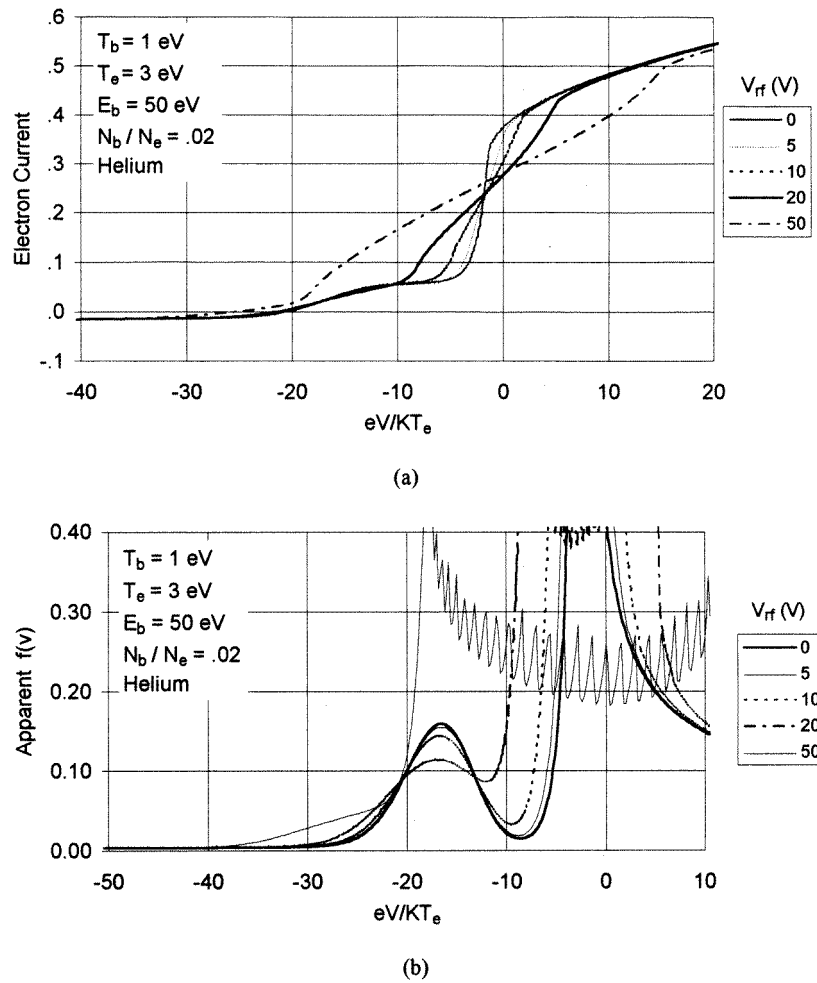$$dJ_b/d\eta = f h^{-1} \exp[-(\sqrt{-\eta}/h - q)^2]. \qquad (39)$$

Figure 14. (a) Uncompensated probe characteristics for a 3 eV plasma with a phased beam and various levels of RF pickup. (b) Apparent distribution functions derived from (a). The rapid oscillations are due to the coarseness of the numerical grid and should be ignored.

Although the maximum of this curve occurs at the expected potential, the e-folding points of the curve are separated by $\Delta\eta = 4qh^2$, a factor $q \gg 1$ larger than the width of $2h^2$ of the original energy distribution. The beam distribution, as it would appear when plotted against probe potential, is shown in figure 7 for various beam temperatures and velocity shifts. The distribution seems to widen as it is accelerated, but this is because $\partial J/\partial\eta \approx f(v)$ is plotted against v^2, not v.

For the constant-energy case, the peak of the beam occurs at the probe potential corresponding to the energy gain (figure 8), but the width of the beam narrows (in velocity space) as W is increased (figure 5). Since $f(v)$ is no longer Gaussian, the width of the observed $f(v)$ depends on how well the singularity is resolved. With good resolution, a probe might yield the $f(v)$ curve shown in figure (8), which was computed from equations (33), (35), and (38) with a grid size $\Delta\eta = 0.1$. The width appears to be less than $T_b = 1$ eV, illustrating the well known effect of acceleration cooling. A coarser grid
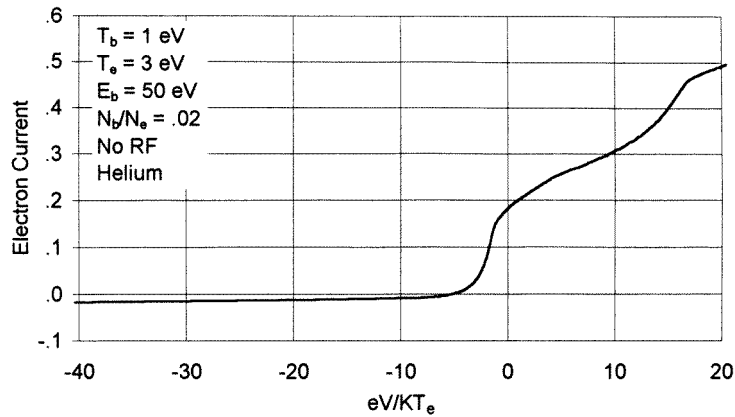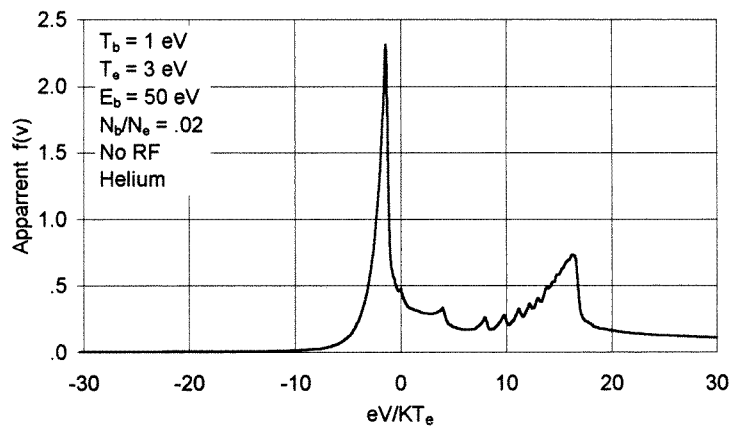
Figure 15. (a) *I–V* characteristic of a V_f-compensated probe in a 3 eV plasma with a pulsed, 50 eV electron beam. (b) Apparent $f(v)$ from the derivative of (a).

or probe resolution would give, however, a wider apparent $f(v)$. Figure 9 compares the apparent $f(v)$'s for two types of beam, one with constant-velocity acceleration and the other with constant-energy acceleration, both starting with the same temperature T_b and suffering the same mean energy gain E_b. It is clear that the apparent widths can be very different.

4. Computed probe curves

In this section we use the formulae of sections 2 and 3 for computations illustrating the effects of RF fluctuations, fast electron populations, phased beams, and V_f compensation on probe *I–V* curves. To permit the ion saturation current to be seen, we have increased it by choosing a light ion, namely He, in all the calculations. We have also simplified the calculation by choosing a shifted Maxwellian for the beam electrons.
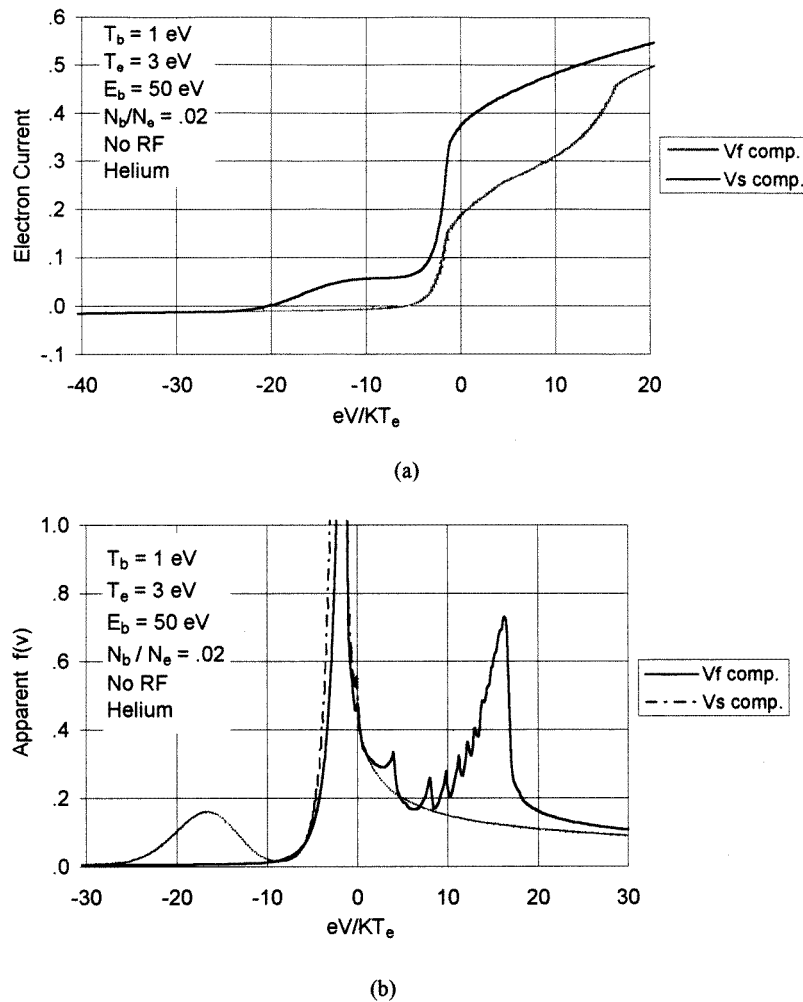
Figure 16. (a) *I–V* curves for probes driven to follow V_s and V_f in a plasma with a phased beam. (b) Apparent $f(v)$'s derived from (a).

4.1. Effect of RF pickup on dc beams

Figure 10(a) shows the model probe curve given by equations (15), (12), (14), and (22). Figure 10(b) shows how the *I–V* curve, averaged over an RF cycle, is distorted by varying magnitudes of V_{rf}. This behaviour is in general agreement with results published earlier by Hershkowitz [5] and others. In practice, the RF potential fluctuation in the plasma can be as large as several hundred volts; in this case, V_{rf} represents the amount of RF pickup remaining after attempts to eliminate it. Figure 10(c) shows the apparent velocity distribution $f(v)$ obtained by differentiating the curves in figure 10(b). Even 5 V of uncompensated V_{rf} is sufficient to distort the Maxwellian distribution beyond recognition. In figure 11, the effect of adding a dc beam of varying density n_b, temperature T_b, and centre energy E_b is shown. In figure 12(a), the effect of RF on a probe curve with a dc beam is shown. The apparent
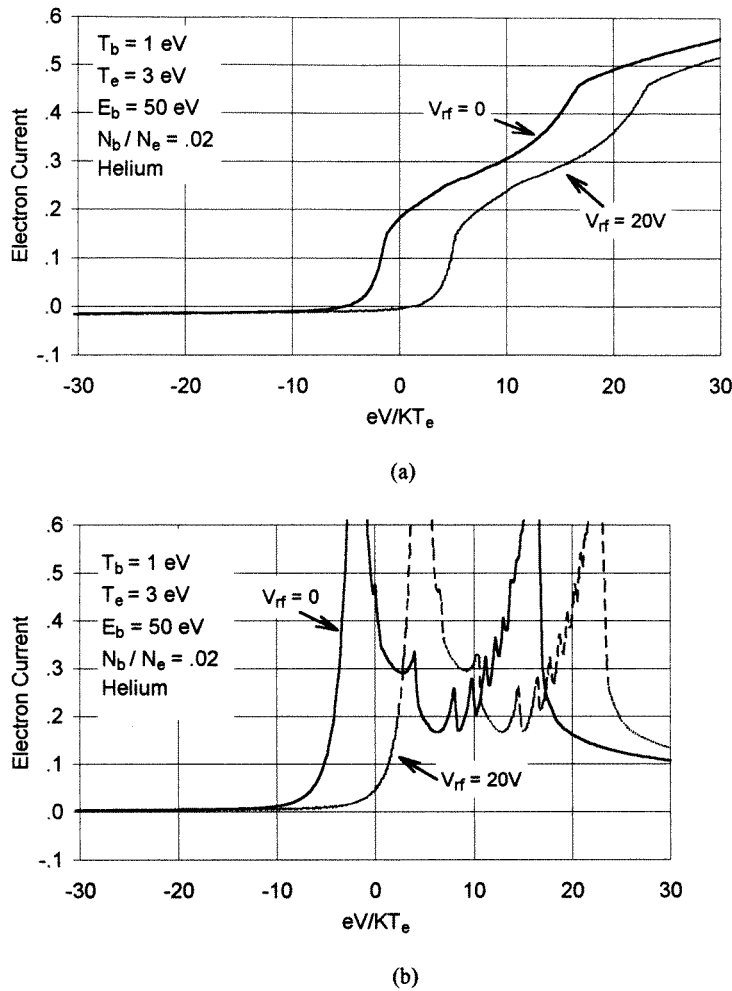
Figure 17. (a) I–V characteristics for V_f-compensated probes in a plasma with a phased beam, with $V_{rf} = 0$ and 20 V. (b) Apparent $f(v)$'s derived from (a).

$f(v)$'s for the thermal part of the distribution is indistinguishable from figure 10(c), but the high-energy portion (figure 12(b)) shows the presence of the beam with the correct central energy even with V_{rf} as large as 20 V.

4.2. Phased beams

We now consider electron beams which occur only during the accelerating phase of the RF cycle. Figure 13(a) shows the assumed time variation of the beam, and figure 13(b) the probe characteristics for various values of the maximum beam density. Figure 14(a) shows the effect of RF pickup on one of these cases, and figure 14(b) the corresponding distribution functions derived therefrom. Note that the beam can be detected as long as V_{rf} is less than E_b.
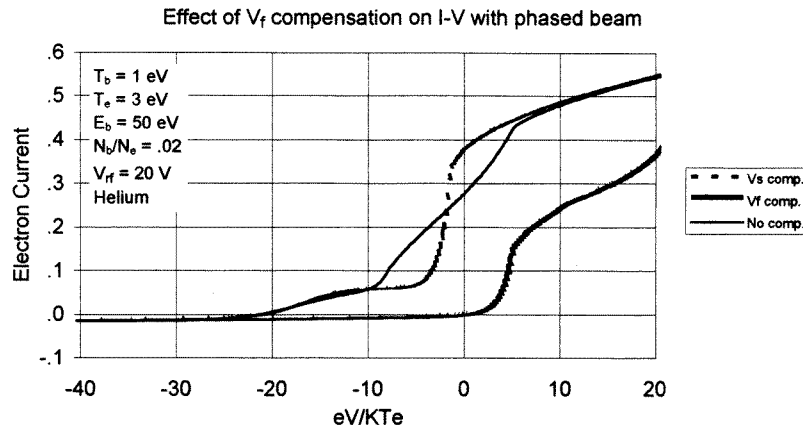
Effect of V_f compensation on I-V with phased beam

Figure 18. I–V characteristics for a probe in a plasma with a phased beam and $V_{\rm rf} = 20$ V, for cases of no RF compensation, $V_{\rm f}$ compensation, and ideal $V_{\rm s}$ compensation.

4.3. Effect of $V_{\rm f}$ compensation

Figure 15(a) shows the time-averaged characteristic for a probe in a plasma with a phased beam in the absence of RF pickup, but with compensation circuits designed to follow fluctuations in floating potential. This curve was computed by shifting the I–V curve at each RF phase so that the floating potential occurred at the same probe potential as it did when the beam current was zero. The derivative of this curve gives the apparent distribution function shown in figure 15(b). We see that the oscillation in floating potential causes $f(v)$ to be smeared out, as if there had been RF pickup. Figure 16 compares these curves with the ideal curves which would be obtained in the absence of both RF and RF compensation, or in the presence of RF pickup but with ideal compensation following the fluctuations in space potential $V_{\rm s}$. In figure 17(a) we compare the curve of figure 15(a) with the curve obtained with 20 V of uncompensated RF. Figure 17(b) shows the derived distribution functions. Since the characteristic has already been distorted by $V_{\rm f}$ compensation, the further addition of RF pickup has only the effect of shifting the curve. Finally, in figure 18, we compare the probe characteristics with RF pickup and a phased beam for the cases of no compensation, $V_{\rm f}$ compensation, and ideal $V_{\rm s}$ compensation. We see that the presence of the beam cannot be detected with $V_{\rm f}$ compensation.

Acknowledgments

References

[1] Chen F F and Chevalier G 1992 *J. Vac. Sci. Technol.* A **10** 1389
[2] Chen F F 1991 *Plasma Phys. Control. Fusion* **33** 339
[3] Ellingboe A R, Boswell R W, Booth J P and Sadeghi N 1995 *Phys. Plasmas* **2** 1807
[4] Sudit I D and Chen F F 1994 *Plasma Sources Sci. Technol.* **3** 162
[5] Hershkowitz N 1989 *Plasma Diagnostics* vol 1, ed O Auciello and D L Flamm (New York: Academic) ch 3
[6] Tonks L and Langmuir I 1929 *Phys. Rev.* **34** 876